Towards Optimization of ECG noise Suppression in Adaptive Deep Brain Stimulation

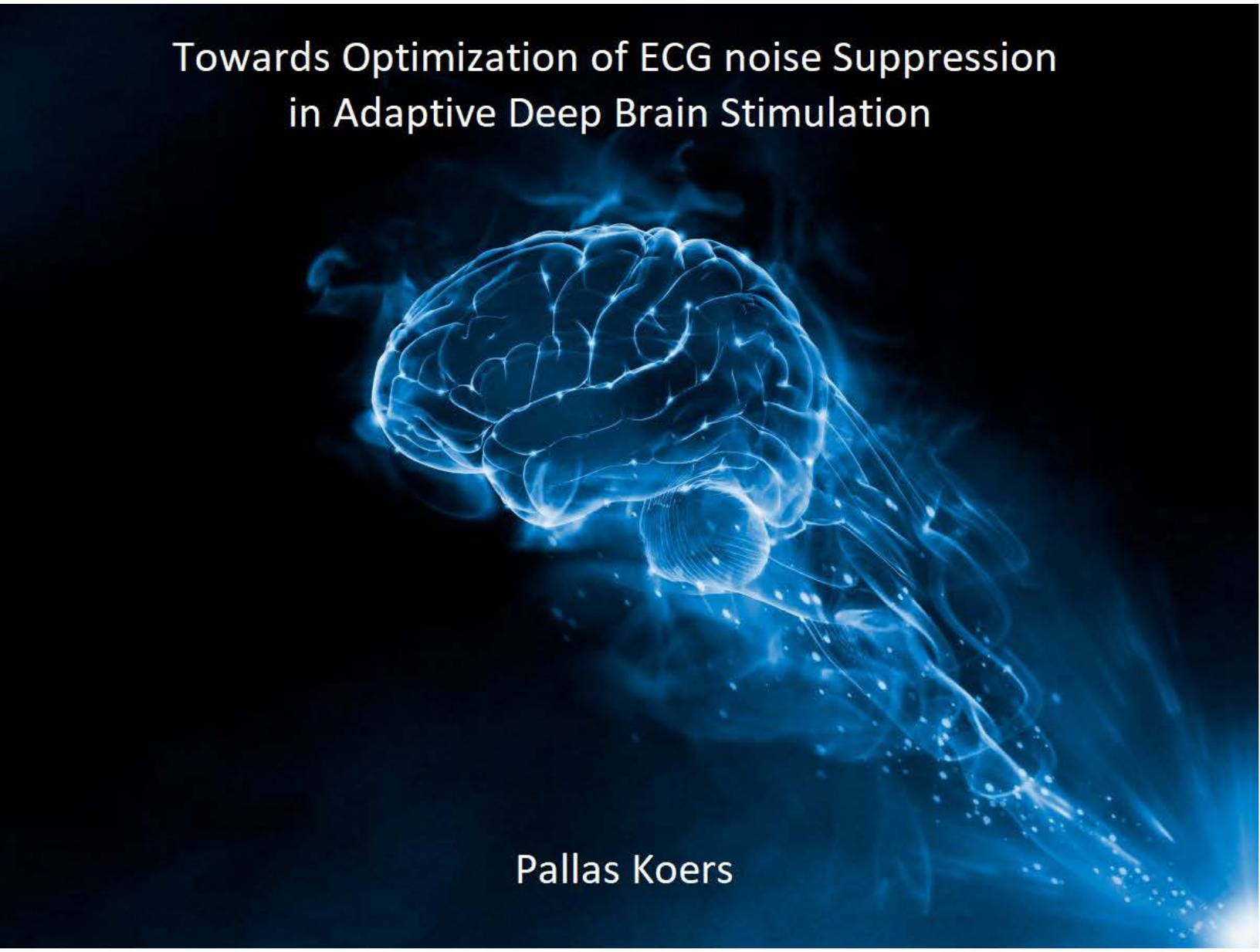

Pallas Koers

TU Delft

Amsterdam UMC
Universitair Medische Centra

Towards Optimization of ECG noise Suppression in Adaptive Deep Brain Stimulation

Pallas Diana Lotte Koers

A thesis presented for the degree of
Biomedical Engineering, track of Bioelectronics and Medical Devices to be defended publicly on 02-02-2022 at 09.00 AM.

3ME / Circuits and Systems / Amsterdam UMC

Delft University of Technology

Student number : 5090156

Thesis Committee Chair: Wouter Serdijn

Thesis Committee Member: Justin Dauwels

Thesis Committee Member: Martijn Beudel

ACKNOWLEDGEMENTS

At the beginning, I would like to contribute my acknowledgements to the people that have been important for the final result of this thesis.

First of all I would like to thank my supervisor Justin Dauwels, for your guidance and mentorship during this project. Your sharp eye has both pushed me to get to most out of myself and challenged my way of problem solving. Without you, I would not have had this current knowledge regarding signal processing and programming. I always felt that there was time and room for discussing my progress and that, especially in times of COVID-19, has been very welcoming. I am happy to have had you as my supervisor.

Secondly, I would like to thank the Percept Research Group at the Amsterdam UMC. In hindsight, stepping into the world of neurological signal analysis as been a great learning curve. It has been great to have the possibility to brainstorm about the many questions that are still unanswered in this field of study. In particular, I would like to thank Dr. Martijn Beudel, for providing me with the trust and opportunity to work on this extraordinary project. Your passion for this field has been very motivating and I thank you for your mentorship during this time.

Thirdly, I would like to thank Mariëlle, for being a real support during this time on various levels. It has been a pleasure to brainstorm with you about how to handle signal processing issues. It has been great to see your enthusiasm for this field and I am happy to follow your findings on your way to your PhD.

Fourthly, I would like to thank you Grachi for your support with my technical questions.

Lastly, as this thesis is the end of a great student time, I would like to thank all the friends that I have made on the way. My time in Groningen will have a special place in my heart. I look back with great joy and laughter and inspiration for the next phase in life.

I dedicate this thesis to my family and friends for always supporting me. To my mother, who I lost at the age of 17, I know you would be cheering for me. And last but not least my grandmother, who never had the opportunity to study pharmacology. For her, I am grateful to see the tides have turned.

PREFACE

This study was conducted under the joint supervision of Justin Dauwels from the Department of Microelectronics of the Delft Technical University and Dr. Martijn Beudel of the Department of Neurology at the Amsterdam UMC. Due to COVID-19, most of the work on this thesis had to be done at home. In hindsight, this experience has challenged my self-discipline, creating a good focus in times of uncertainty and reaching out for appropriate guidance on time.

The basis of this thesis originates from my passion for Biomedical Engineering. I have always been enthusiastic about nature, technology and the human touch. Since the age of 14, I knew that the study Biomedical Engineering would be the perfect combination of these interests. And at the end of my study, I can confidently say that I still feel very fortunate to live in the time where this study is still so fascinating.

My time at Second Sight Medical Products has further triggered my interest in the field of bioelectronic medicine. It was extraordinary to be able to observe patients that were able to see again due to a camera and retinal nerve stimulation. After this, I was certain I wanted to know more about bioelectronics.

As both my grandfathers has suffered from Parkinson's Disease, it has been an honour to work on the development of this technology. The most remarkable moment of this internship has been seeing Parkinson's Disease patients before and after Deep Brain Stimulation, in a time window of 30 minutes. This image will surely stick with me. And I am thankful for the opportunity to have seen what this technology can truly do in real-life.

The next decade will be captivating for deep brain stimulation research due to rapid advances in technology. I am happy to say that the future offers a positive perspective to both the current and next generation Parkinson's Disease patients.

NOMENCLATURE

ABBREVIATIONS

Abbreviation	Definition
DBS	Deep Brain Stimulation
aDBS	Adaptive Deep Brain Stimulation
PD	Parkinson's Disease
LFP	Local Field Potential
ECG	Electrocardiogram
std	Standard deviation
Fs	Sample Frequency
NLMS	Normalized Least Mean Squared
FDA	Food and Drug Association
STN	Subthalamic Nucleus
GPi	Globus Pallidus
IPG	Implanted Pulse Generator
EEG	Electroencephalogram
BPM	Beats Per Minute
PSD	Power Spectral Density

SYMBOLS

Symbol	Definition	Unit
V	Voltage	[kg*m^2*s^{-3}*A^{-1}]
η	Step size	

Contents

Abstract*—Adaptive Deep Brain Stimulation (aDBS) offers the potential for personalized stimulation strategies for patients with Parkinson's Disease (PD). The closed loop characteristic of this system requires the incorporation of PD relevant biomarkers that determine the patient's need. In order to obtain high quality LFP (Local Field Potential) input signals, the ECG (electrocardiogram) noise should be suppressed. The aim of this project is to study the performance of various algorithmic ECG noise suppression methods. Out of the ADAPT-PD trial, we have taken 9 LFP channels with consistent ECG artefacts for exploring the performance of ECG noise suppression models. As a reference point for filtering performance, we have used survey data (DBS-OFF). Using an externally measured ECG as reference, we have implemented two Adaptive NLMS (Normalized Least Mean Squared) Noise Cancellation algorithms. For the first version, we have used stimulation ramping alone for synchronization of the data sets. The second version includes an extension that aims to improve only the data synchronization feature. Furthermore, we have explored the ECG noise suppression performance of a proposed template subtraction method, using 11 different variations of epoch length. For improved analysis, we have used three data sets, namely personal (#1), patient group (#9) and simulated (#5346) data, using the Perceive toolbox as the benchmark. Simulated LFPs are based on survey data combined with 9 external ECGs in 11 levels of contamination (100-1100%). We have conducted analysis in both the time and frequency domain (beta-range), in order to estimate the absolute difference from the reference survey. Outcomes in the frequency domain show that, for personal performance, template subtraction tweaking provides an improvement up to 37.6 % over the Perceive toolbox. Furthermore, the outcomes show that, for both the patient and simulation group, optimal performance is obtained using the Perceive Toolbox with 20.7 % accuracy for the patient group and 4.7 % for the simulations. It can be concluded that the survey LFPs can be used for personal calibration of ECG noise suppression. This contradicts the aim to find one universal LFP ECG noise suppression method. There is a need for a reliable data synchronization method between the Percept^{TM} LFPs and other biometric data. Reliable synchronization would improve the usability of the external ECG as reference signal in adaptive filters. Furthermore, reliable synchronization would accelerate the discovery of linked physical symptoms for Parkinson's Disease biomarkers.

1. Introduction

Over the past 30 years, DBS has proven to be an effective treatment for patients with PD who show an inadequate response to medication alone. PD is a chronic neurodegenerative disorder characterized by tremor, stiffness, postural instability and loss of facial expression [1]. For PD, DBS has been the most important therapeutic improvement since the development of levodopa medicine. DBS was first FDA approved in 1997 as a therapy for tremor, and later in 2002 for general PD. Currently, over 160.000 patients worldwide have been treated with a DBS implant for treating PD related symptoms [2].

In order to control normal body movements and other functionalities, neurons communicate using electrical signals. In the brain of PD patients improper folding of proteins is observed. This results in a chain reaction of progressive protein folding and clumping, which has been linked to damage of neural communication [4]. DBS delivers small electrical pulses to a targeted brain area in order to disrupt the abnormal neural communication [5]. The exact mechanism behind the DBS induced reaction chain is still unclear, but researchers assume dopamine to play a major roll. After DBS, increased levels of dopamine have been observed in the STN of PD patients. Increased dopamine levels have been linked to decreased PD motor symptoms [6].

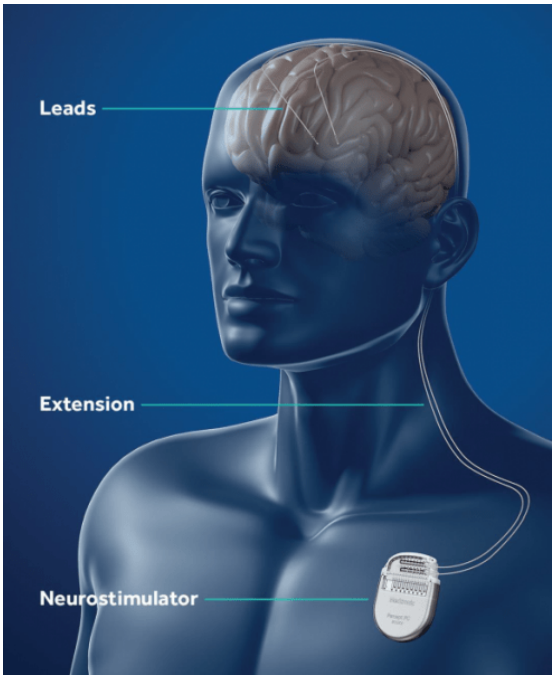

Figure 1: Illustration of the Percept DBS system. An IPG is placed above the heart. The stimulated pulse travels through the leads extension towards the leads situated at the STN or GPi. Image taken from [3].

For PD patients, the STN and GPi are the common brain areas for bilateral electrical leads placement [7]. These leads are connected to the IPG that is normally placed above the heart, similar to a cardiac pacemaker (Fig. 1). This IPG includes a battery and generates the electrical current that is delivered at the targeted brain area via the lead's electrodes.

Due to the limited knowledge of the exact neural chain reaction of DBS, the stimulation strategy provided to the PD patient is still based on subjective assessment of a clinician. Calibration of the stimulation parameters such as frequency, pulse width, voltage and current amplitude is done by the clinician, taking the clinical outcome and unwanted side effects into account. Headache, confusion, problems with vision or speech, numbness or tingling sensations are unwanted side effects that have been documented after DBS stimulation. Moreover, higher stimulation voltages have been linked to neuro-psychiatric symptoms such as severe depression, mood changes and impulsive behaviour [8].

The IPG has a specific battery longevity related to stimulation strength and frequency. A surgical replacement of

the IPG is needed every 10-15 years, affecting the patient's quality of life. Therefore, a trade-off should be made between the stimulation dosage and clinical outcome, considering the battery longevity [9]. In general it has been observed that DBS clinical efficiency attenuates over a period of 6 months, using a consistent stimulation dosage [10]. The amount of subjective clinical assessments is trade of between parameters optimization, costs, time and patient discomfort [9].

In 2020, the Medtronic Percept^{TM} aDBS system was approved for aDBS trial for patients with PD. The Percept is the first FDA approved fully implanted aDBS system with BrainSense^{TM} technology and stimulation. This aDBS system both stimulates and measures brain activity at the same time. In the future scope, this real-time feedback loop could be used to provide stimulation based on a patient's need. Compared to conventional DBS, that applies stimulation permanently, this aDBS system opens up personalized treatment perspectives.

This potential demand and supply behaviour of aDBS aims for optimal clinical outcomes, whilst both reducing DBS induced side effects [11] and maximizing the battery longevity. Additionally, a given battery will last longer, minimizing surgical replacements. This reduces the risk of surgical complications such as infection and severe tissue damage.

Brain activity for the aDBS system is measured as LFPs, representing the activity, defined as the difference between electrode points, of a few neurons. This is different from prior common EEG recordings, that require multi-channel recordings with various electrodes placed on the scalp. Therefore this new BrainSense^{TM} technology provides for the first time, local insight in a neural response to a stimulation strategy [12].

In order to translate the captured LFPs into a clinical state, PD specific biomarkers need to be incorporated into the aDBS system. A biomarker is a measurable and reproducible medical indicator used as an objective prediction of a persons clinical state. However, qualitative identification of biomarkers and translation into aDBS algorithmic strategies is yet to be achieved. This section highlights the ECG artefacts found in LFP recordings and their limitations for quality neural feedback in aDBS systems.

The quality of the input signal is crucial for the accuracy of the feedback and clinical performance of aDBS. Real-time LFP recordings are prone to various artefacts such as cable, stimulation or ECG artefacts [13]. As the contraction of a heartbeat is the strongest electrical activity of the body, it can be observed as an ECG artefact throughout LFP recordings [14]. In the following section, the general waveform of the ECG will be elaborated. Next, its interference with the PD brain activity of interest will be highlighted.

A. ECG in general

A common ECG has a distinct waveform consisting of a P wave, QRS-complex, ST segment, T wave and U wave

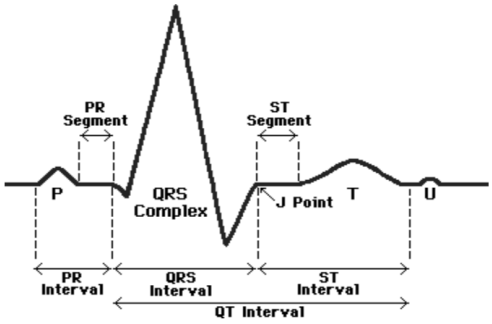

Figure 2: Illustration showing the ECG-complex with its characteristic P-wave, QRS, T and U wave. Illustration taken from [16].

(Fig. 2). The interval between an R wave and the next R wave is around 0.8 seconds, depending on the BPM. Groups of specialized cells in the heart control the phases of the heartbeat by causing electrical potentials. The total ECG-complex includes:

- P wave: electrical impulse is conducted from the sinoatrial node, the main pacemaker of the heart, initiating a heart beat by generating the electrical impulse. This pulse travels towards the atrioventricular node and spreads from the right to the left atrium. This depolarization (contraction) of the atria results in the P Wave in the ECG [15].

- QRS-complex: The QRS-complex is the result of rapid depolarization of both ventricles. As these contraction muscles are bigger than the atria contraction muscles, this amplitude is larger than the P wave.

- T wave: Ventricular repolarization results in the prior ST segment and the T wave.

- U wave: The U wave represents the last wave of ventricular repolarization.

B. Frequency overlap and Biomarkers

Research has been focused on finding PD specific biomarkers in the time and frequency domain of brain signals. LFPs resemble oscillations of frequencies including delta and theta bands (1-7 Hz), alpha and beta band (8-30 Hz), gamma band (30-200 Hz) and higher frequency oscillations above 200 Hz. PD patients are characterized with the presence of increased activity in the beta range (13-30 Hz), i.e. the 'beta-peak'. This beta-peak is linked to bradykinesia and rigidity and is used as a PD biomarker [17]–[19].

An overlap in the frequency spectra of both LFP and ECG signals suppresses this beta-peak, resulting in an inadequate

biomarker identification. Fig. 3 shows a positive relation between the presence of ECG and the suppression of a beta-peak (13-Hz). Classical digital filters such as low and high-pass or band pass filters can not be used to extract the desired signal due to the overlap of these frequency bands [20].

Due to the novelty of LFP recordings, most methods are based on EEG multi-channel input, making them inadequate for LFP filtering. These artefact suppression methods range in complexity, applicability and computational demand [21]. For real-time aDBS with LFPs, an ECG noise suppression method should be proposed that is low in neural information loss, high in accuracy and low in computational demand.

C. Perceive Toolbox

Recently, an extension was added to the open-source Perceive Toolbox enabling the removal of ECG artefacts out of the LFP signals [23]. This Perceive extension is based on applying cross-correlation over sliding windows, generating a recording specific template of ECG artefacts. Subsequently, segments of signals affected with ECG artefact are identified by using pattern matching. Afterwards, the identified segments are replaced by mirrored padding. Fig. 3 shows the result of ECG artefact removal by use of this novel Perceive Toolbox in the time and frequency domain.

D. Template Subtraction 100

Research conducted by the Amsterdam UMC Neurology department documented a different ECG noise suppression approach [22]. Their algorithmic method detects ECG artefacts in the LFP signal, creating a QRS-complex template for every found R-peak, optimized in both scale and offset. The QRS-complex epochs are averaged to find a LFP channel specific ECG artefact template (green line) (Fig. 4). The tails of the epochs are deflected to an equal value, preferably zero. Within every epoch of the LFP, this QRS-template is subtracted as per formula (1).

$$LFP_{filtered}(QRS) = LFP(QRS) - LFP_{ecg}(QRS) \quad (1)$$

E. Problem Statement

The documented Amsterdam UMC template subtraction method uses a defined epoch length of 100 samples, resembling 0.4 seconds with 250 Hz sampling rate. The length of this epoch has been arbitrarily chosen and variations have not been explored. Presumably, as the deflection step is based on the epoch length, variations could influence the shape of the LFP Zero-Template and thus the filtered LFP. Thus the variations in algorithmic performance can be analyzed.

As compared to above method, aDBS requires the usage of filter algorithms that rapidly adapt to feedback changes. Adaptive filters are known as a robust and simple processing method that has been implemented for various noise cancellation problems. However, implementation of adaptive filters for LFP data is still to be examined. Furthermore, the availability of the external ECG provides next to the LFP, provides new research possibilities. It could be explored whether the usage of the ECG as an extra reference for ECG artefacts removal is beneficial for LFP signals.

BrainSense^{TM} technology provides the availability of survey data which are LFPs free from ECG artefact [24]. Survey data characteristics will be explained in the method section. Yet, usage of this data as an extra reference signal could be investigated. Even though researchers have been focused on finding a universal golden standard method for ECG noise suppression, it is presumed that survey data could be incorporated for a personal tweaking of ECG noise suppression filters.

F. Goal

In order to close this research gap, various algorithmic approaches should be examined for their ECG noise suppression performance. The scope of this paper entails the implementation of adaptive noise cancellation filter and variations of the template subtraction method. Results of the Perceive Toolbox will be included for comparisons. Furthermore, the benefit of ECG and survey LFP as reference signals for ECG noise suppression will be investigated. The aim of this research is to obtain optimal performance of ECG noise suppression in LFP data both on patient and patient group level, enriched by simulations. Moreover, the influence of epoch variations on its ECG noise suppression performance will be assessed.

Summarized, as only qualitative LFPs can be used for real-time personalized stimulation strategies, ECG noise needs to be removed. Because only a few LFP specific ECG artefact filtering methods exist, various approaches can still be explored. As an example, the usage of ECG as the external reference in noise cancellation method could be assessed. The aim is to explore adaptive filters and epoch variations on their performance of ECG noise suppression.

2. Methods

In this section, the methods used for the scope of this project are outlined. First, the included patients and data collection protocol will be discussed. Secondly, research circumstances will be highlighted such as the types of data collected, prior data synchronization, inclusion of data, electrode pair characteristics and data preprocessing. Thirdly, the working mechanisms of created and adjusted ECG noise suppression algorithms will be explained. Decisions for the implementation or adjustments during the usage of these filters will be highlighted. Lastly, the choices for the analyses of the results will be explained.

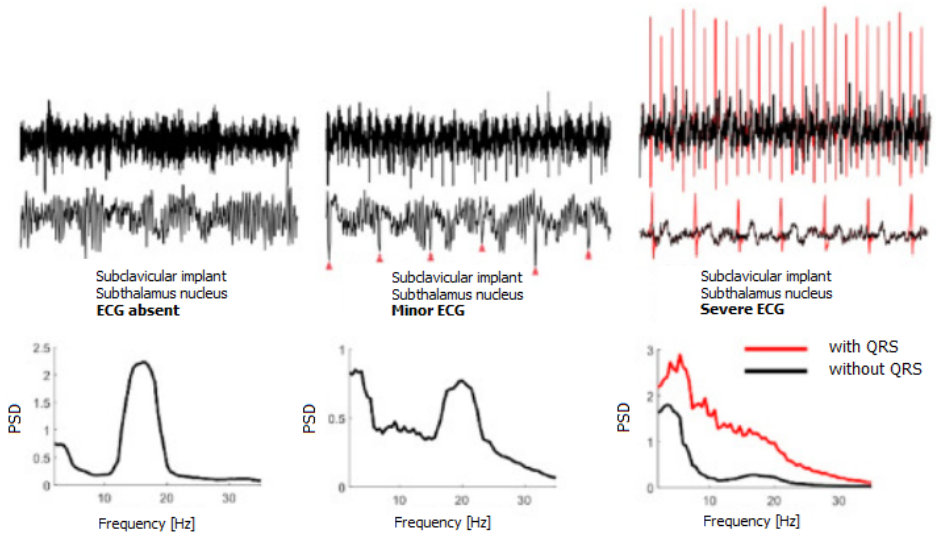

Figure 3: Figure showing the ECG contamination (absent to severe) of subclavicular implants with QRS-complex peaks in the time domain. Below the corresponding PSD for each LFP is shown. On the right side, the PSD with or without QRS-complex is presented. Showing the reappearance of a small beta-peak without QRS-complexes. For these graphs, the ECG filtering was done using the Perceive Toolbox. Graphs taken from [14].

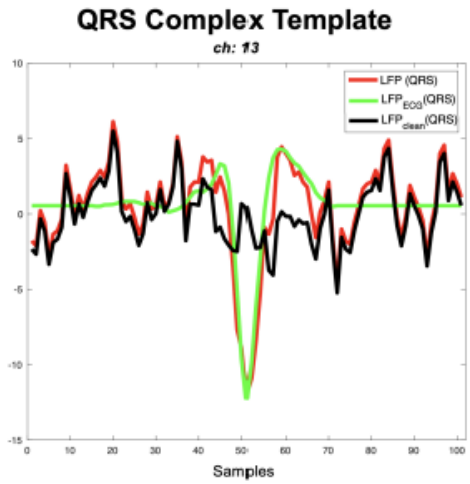

Figure 4: Graph showing an example of a QRS-complex template with an 100 sample epoch width (0.4 s). The red line is equal to the data points of the raw LFP. In green, the QRS-complex template is shown. In black, the outcome of template subtraction can be seen. Graph taken from [22].

A. Research Patients

For this study, we have incorporated participants from the ADAPT-PD (Adaptive DBS Algorithm for Personalized Therapy in Parkinson's Disease) trial. This trial was started in order to evaluate the safety and efficiency of aDBS in patients with PD and covers 12 research centers in Europa, the US and Canada, conducting movement disorders research.

We have included 9 PD patients, all implanted with bilateral electrode leads. The patients were scheduled to replace their IPG with the Medtronic Percept^{TM} IPG. Patients were informed by the details of the data collection and usage by the clinicians. Additionally, the clinicians have instructed the patients to stop taken their levodopa medicine prior to arrival in the hospital. This is to avoid its influence on PD symptom suppression.

Right after leaving the recovery room, we have instructed the patients to conduct the behavioural protocol. This protocol includes both a DBS-OFF and DBS-ON run. Each run entails a period of rest, a period of reading aloud and a period of upper limb movements *(Appendix A)*. Simultaneously to the behaviour protocol, we have recorded LFP, ECG, vibration sensor (on both hands) and video data.

B. LFP Data Collection

The aDBS system measures LFPs in both hemispheres. Each hemisphere has one lead. Each lead contains four contact points. Out of these four contact points, three contact pairs are made. In total six contact pairs are available per patient. These contact pairs have been used to capture both streaming and survey LFP data. Their difference will be explained in the next two subsections.

1) Streaming Data

Streaming LFP data is the LFP data recorded while the Percept^{TM} is on the ON-DBS mode, i.e. an electrical pulse during application of 0 or higher mA. In this case, the LFP recordings are contaminated with ECG artefact. Per patient, only one contact pair can be chosen per hemisphere for recording streaming data. This is because the stimulation is provided by the intermediate contact points. Therefore, we

have captured a total of 18 (9*2) streaming LFP channels for this study.

2) Survey Data

The Percept^{TM} system has the ability to record the LFP signals when the system is switched off, being in the OFF-DBS mode. This provides the possibility to record the bilateral LFPs without any ECG artefact leakage. As survey data can only be recorded in OFF-DBS, this data is inadequate for real-time aDBS feedback.

Survey data can be measured between the 6 contact pairs per patient, given a total of 54 (9 * 6) survey data channels. For this study, we have used 20 seconds of survey data, recorded at the start of the behavioural protocol. For this project, we have chosen to use the survey data as a reference signal for ECG noise suppression performance.

Both streaming and survey LFPs were recorded by the Percept at a sampling rate of 250 Hz. By default, the Percept processes the LFPs with a 1-10 Hz high pass filter and two 100 Hz low pass filters. The LFPs were amplified by 250 times and send wireless to the Clinician Programmer Percept^{TM} tablet (Fig. 5). This tablet was designed to be the only direct receiving unit of the LFPs, in order to protect the patient data. Additionally, real-time captured LFPs and calibration settings can be observed on this tablet during stimulation.

Electrode impedance is a determining factor for both applying and recording a current. Impedance is the resistance to electrical current delivery in an alternating current circuit. Invasive electrode contacts are prone to foreign body reactions, such as scar tissue formation or the attraction of giant cells. [25] These adverse reactions influences the interfacial distance and impedance between the electrode and neurons. Higher encapsulation is related to higher electrode impedance [26], affecting the performance of DBS. Fig 6. illustrates the formation of scar tissue and increased interfacial impedance. The clinician has assessed the various contact point impedances using the tablet programmer. The contact points with the best characteristics were chosen for stimulation and sensing. The streaming and survey LFP channels were exported as a JSON-file and preprocessed with the Perceive Toolbox by the team of clinicians and research students.

C. ECG Data Collection

We have measured the bipolar ECG signal with two electrodes placed on the right and left upper chest during the LFP recording. We have placed a ground electrode on the C7 cervical vertebrae. We have recorded the ECG data at 2048 Hz sampling rate using a TMSi Porti amplifier.

D. Time Synchronization of Data

Notably, a millisecond timestamp for the captured LFPs is not incorporated into the Percept^{TM}. Due to this design

Figure 5: Image showing the Percept IPG (left) the Percept Clinician Programmer Tablet (middle), a Patient Programmer on the phone to track events (right) and an example of implanted electrode leads with various contact electrode points. Image taken from [27].

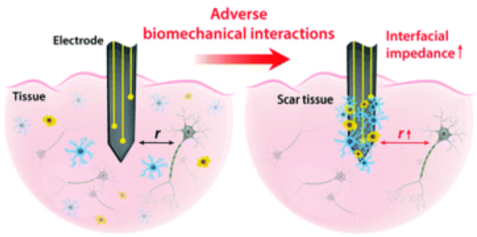

Figure 6: Illustration of the adverse reaction such as scar tissue by the placement of the electrode. These adverse reactions result in increased impedance between the neuron and the electrode, influencing the measured LFP or the received DBS stimulation. Image taken from [28].

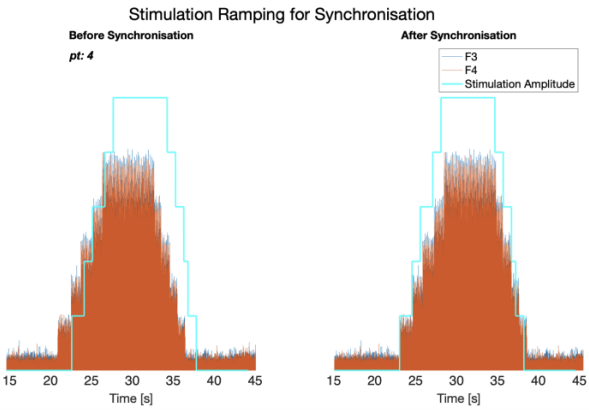

Figure 7: Image showing the stimulation ramping measured at the stimulation artefact electrode. The Blue line shows the stimulation amplitude, of which the shape can be observed in the electrode recording. The shape matching is used to identify the moment of stimulation ramping, in order to synchronize the data. Image taken from [22].

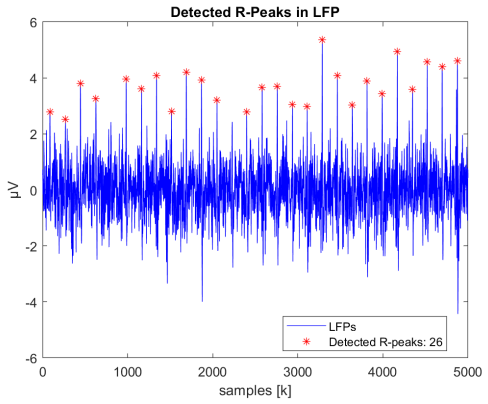

Figure 8: Graph showing an example of a LFP channel (blue) with identified R-peaks (red) in a 20 seconds recording (250 Hz), via the R-peak detection algorithm.

limitation, we have applied an alternative time synchronization approach for the LFP and ECG data. This time synchronization approach, called stimulation ramping, has been proposed by research of the Amsterdam UMC and Oxford University. The method includes the placement of 2, so called stimulation artefact electrodes, on the forehead of the patient. By up and down ramping of the stimulation, a stair effect of signal amplitude change can be visualized on these two electrodes (Fig. 7).

The initial moment of upramping is determined by a threshold set regarding amplitude's rate of change. Then, the Percept data is upsampled to match the TMSi sampling frequency. Afterwards, the TMSi recording is aligned by the determined sample difference.

E. Inclusion of LFP channels

We have analysed 18 LFPs of left and right hemispheres on their ECG artefact consistency using an ECG artefact detection algorithm (Fig.8). First we have identified the R-peaks using two formulas:

1) MinPeakHeight = 2.5 * std LFP (z-scored LFP)
2) MinPeakDistance = 0.5 * Fs

Then, we have included LFPs with a consistent ECG artefact for the scope of this study using two criteria. First, the presence of a R-peak within every three second timeframe. Secondly, the presence of a BPM $>$ 40. Using the corresponding ECG as reference, this ECG artefact detection algorithm showed an accuracy overlap of detected R-peak of 85%. This method identified 7 out of the 18 LFP channels with consistent ECG artefact. After visual inspection we have added 2 more LFP channels, providing 9 LFP channels for the scope of this project.

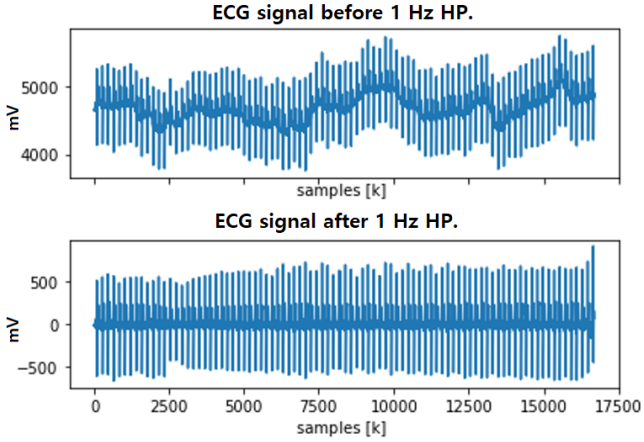

Figure 9: ECG signal before and after 1 Hz highpass butterworth filtfilt, excluding the jumping of signals over time in order to obtain a stable reference signal.

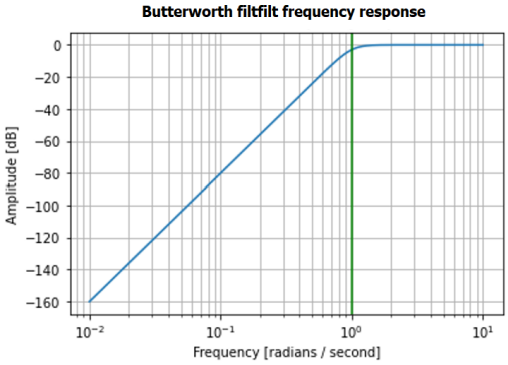

Figure 10: Graph showing the 4th order 1 Hz high-pass frequency response. All $<$ 1 Hz frequency amplitudes are attenuated, providing a 1 Hz highpass filter.

F. Preprocessing of ECG signals

The corresponding ECG signals analyzed showed significant jumping over time (Fig. 9 upper). These disturbances is presumed to be the result of cable off-set, cable and physiological movement which all occur below 1 Hz. Therefore we have implemented a "1 Hz high pass 4th order Butterworth filtfilt" filter on the total length of the raw ECG signal. A Butterworth filtfilt applies a filter twice, once forward and once backwards to a signal, attenuating all frequencies below 1 Hz (10^0) (Fig. 10). After 1 Hz high passing, the ECG showed no longer any jumping (Fig. 9 lower), serving as a stable reference input then. Subsequently, in order to match the length of the streaming and survey LFPs, the stable ECG signal was shortened to 20 seconds.

G. Adaptive Normalized Least Mean Squared

Adaptive filters, being algorithms with self-changing characteristics, are used to estimate a time-varying signal. Compared to usual linear filters, adaptive filters require little or no

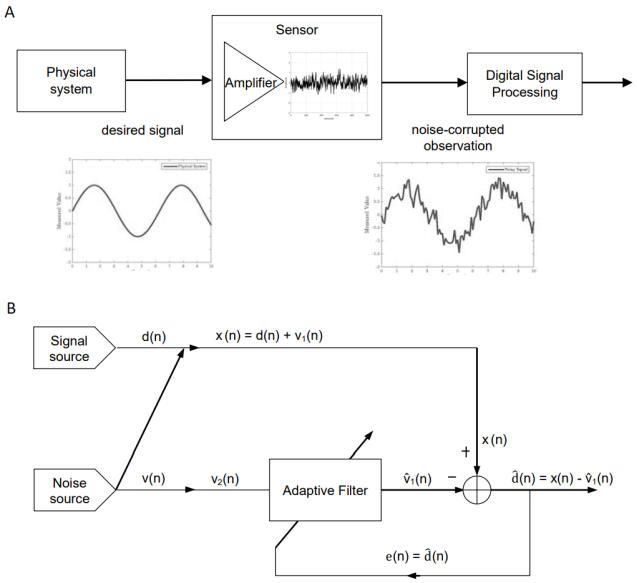

Figure 11: A. Scheme illustrating the denoising principle of a derived signal. A sensor amplifies the signal, after which digital processing is applied to subtract the noise from the noise-contaminated signal. The results is the desired signal. B. of the adaptive noise cancellation principle with reference signal. Where x(n) contains both the desired LFP signal d(n), and ECG noise component $v_1(n)$. The noise estimate $\hat{v}_1(n)$ is subtracted from the signal resulting in desired filtered signal d(n) [29].

knowledge about the signal or noise components. Besides, adaptive filters are more efficient over linear filters when the neural and noise signals overlap in the time and frequency range.

A noise cancellation adaptive filter uses a reference signal to estimate a noise component in the raw, contaminated, signal. Afterwards, it subtracts this estimated noise component from the raw signal in order to obtain a filtered output. Fig. 11a sketches the steps from recording a raw signal towards a filtered signal.

The most frequently used adaptive filter is the LMS (Least Mean Squared) filter. LMS filters use, within a preset step size, a gradient to estimate the time varying signal. NLMS is an extension to the LMS method filter by including a time varying step size η. This time varying learning rate improves the convergence speed of the adaptive filter. The rate of convergence is defined as the amount of calculation and adaptation cycles required for the algorithm to converge to a steady-state or optimum.

For the adaptive noise cancellation filter with a reference signal, the input LFP x(n) contains both the desired LFP signal d(n) and ECG noise component $v_1(n)$ (Fig. 11b). In this scenario, the known reference ECG signal $v_2(n)$ is uncorrelated to the raw LFP signal but, however correlated to the noise component $v_1(n)$.

The reference signal $v_2(n)$ is used to produce a noise estimate $\hat{v}_1(n)$ component within the raw LFP signal. The estimated noise component is then subtracted from this raw signal, generating the desired filtered signal d(n). In order to minimize the output power E, the constant feedback of component estimation is used to adjust the filter weights.

Within the adaptive noise cancellation principle, the systems output serves as the input error signal for adaptive feedback. For this research, we have implemented the NLMS adaptive noise cancellation filter of the PADASIP Toolbox. We have used normalized ECG and LFPs as input signals and an η of = 0.001 [30] *(Appendix. B)*.

Fig. 12a shows an example of normalized LFP of one of nine included LFP signals and corresponding normalized ECG in Fig. 12b. At Fig. 12c an overlay of both signals is created to compare the signals in time.

Even though visual inspection of the Fig. 12c, including the LFP and ECG, seems to show an overlay of peaks, Fig. 12D shows a small mismatch in peak time synchronization.

Fig. 12e shows the estimated noise component n (green line) within the target LFP d (red). The peak mismatch of d and n can also be seen in a focused range in Fig. 12f. After subtraction of the noise component, Fig. 12g shows the estimated desired signal in pink. It illustrates still clearly present ECG R-peaks.

These observations suggested that the stimulation ramping in itself was inadequate for ECG and LFP data synchronization.

H. Synchronization by Autopeak Delay Detection

In response to the mismatch in peak synchronization, we have implemented an extra algorithmic synchronization step. This Autopeak extension aims to calculate the average peak delay that can then be used for data aligning and synchronization.

Autopeak identifies, with a threshold set at 2 V, the locations of the R-peaks in the ECG signal. Around every R-peak location, an equally distributed epoch of 40 samples was saved. Within each of these epochs, the x values of the corresponding R-peak were identified in the LFP signal (Fig. 13). The average distance between the real ECG R-peak and the identified LFP R-peak was calculated and used as a data alignment factor. As the NLMS filter requires equal input values, the signals were cropped to an equal length. The original adaptive algorithm is further referred to as Zero-Delay. The extended adaptive algorithm is referred to as 'Autopeak' (Appendix. B).

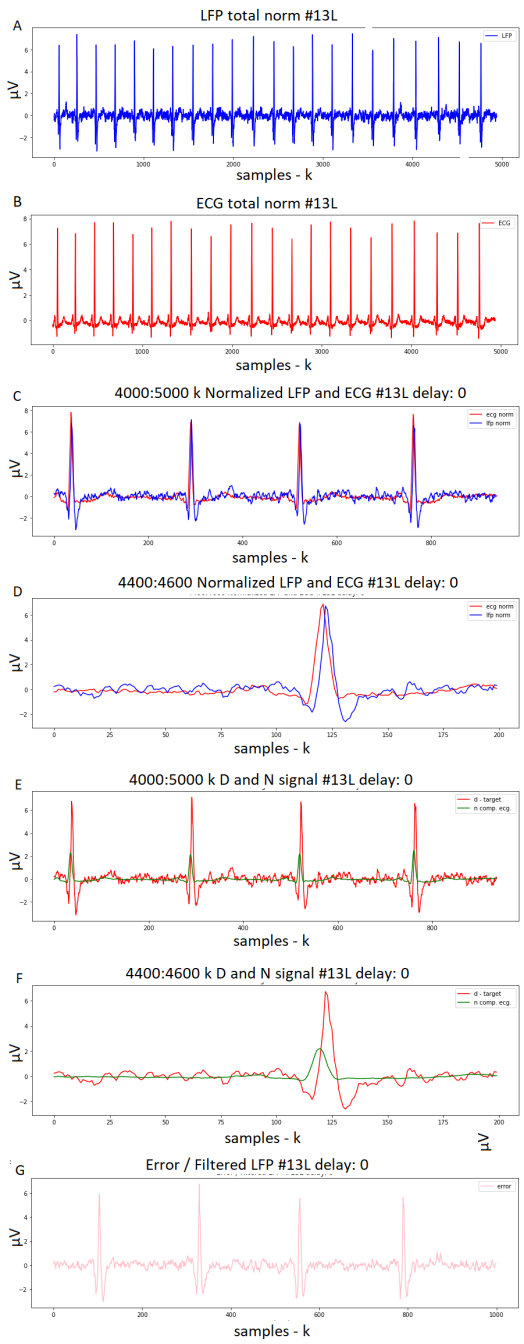

Figure 12: Figure showing example of time plot prior and after NLMS Adaptive Noise Cancellation. A) LFP signal showing consistent artefacts over a long time window. B) ECG signal showing repetitive peaks over a long time window. C) Zoomed-in time window of a normalized overlay of the LFP and ECG signals showing resembles of R-peaks. D: Zoomed-in time window of a normalized overlay of the LFP and ECG signals, showing a slight mismatch in peak time synchronization. E) Raw LFP signal (d) and estimated ECG noise component (n). F) Further zoomed-in time window of the raw LFP (d) and estimated ECG noise component (n). G) Outcome of the d-n subtraction, and the estimation of filtered LFP signal.

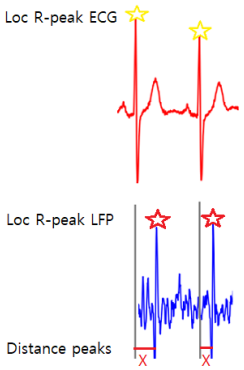

Figure 13: Illustration outlining the Autopeak method. The R-peaks are identified in the ECG and their locations are used to calculate the average distance (x) between the identified ECG and LFP R-peaks.

Compared to the Zero-Delay, the Autopeak time domain data and components show an increased overlap accuracy of the QRS- complex peak, as can be seen in Fig. 14B. Moreover, no significant difference for the n component could be found between Zero-Delay and Autopeak, as can be seen in Fig. 14C. Focusing on a smaller time window, roughly the same d and n peak difference can be observed. Thus, the Autopeak filter output error shows no further improvement in ECG artefact suppression in the time domain.

I. Template Subtraction Variations

The time synchronization method required for the ECG reference methods has disadvantages. Signal processing wise, it is considered to be difficult to ensure qualitative peak overlay due to the steep R-peaks. Furthermore, because of cabling and increased system size it causes patient discomfort.

The template subtraction method overcomes these concerns. Time stamp synchronization is not required. For filtering the timestamp of R-peak found in the LFP is used.

Therefore, for the further scope of this project we have chosen to look into further improvement of the Amsterdam UMC template subtraction model.

For the remainder of this report, we have used this Amsterdam UMC template subtraction method as a baseline, enriching it with 10 algorithmic variations. The resulting 11 approaches, combined with the 2 adaptive filters, are compared with the benchmark, being the original template subtraction method and the Perceive toolbox.

The 11 variations all have a different epoch range ranging from 50 samples to 150 samples in discrete steps of 10 samples.

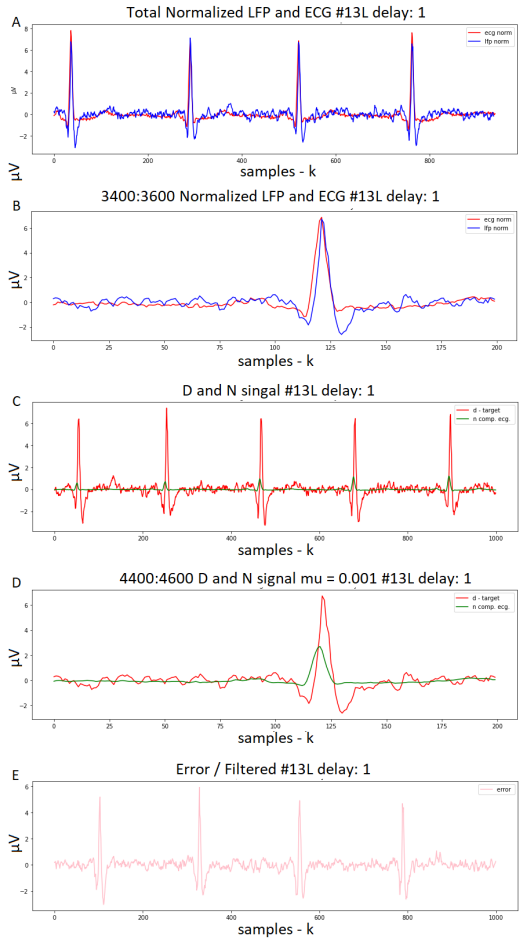

Figure 14: Image showing an example of Autopeak signal filtering. A) Shows the overlay of LFP and ECG signals. B) Zoomed-in time window of the normalized overlay of LFP and ECG signals, showing a slightly better peak time synchronization than with zero delay in Fig 12-D. C) The estimated ECG noise component (n) (green colour) in the raw LFP (d). D) Further zoomed-in time window of noise component (n) (green colour) in the raw LFP (d) (red colour). E) Outcome of the Autopeak LFP signal, showing high amplitude QRS-complexes that are still present in the filtered LFP.

In Fig. 15, for each variation, the QRS-templates are plotted taking an a single LFP channel as an example (Patient 15 right hemisphere). The black line shows the average epoch measurements around every R-peak. A superimposed template is constructed by optimizing the scale and offset using a minimized squared error. Averaging these superimposed templates results in a LFP channel specific QRS template depicted in blue. Further improvement is obtained by an end tail deflecting method, striving for similar end values with preferably zero amplitude. This is referred to as the 'Zero-Template' depicted in green.

Overall, it can be observed that the shape of the Zero-Template QRS-complex is different for every template variation. For example for the right hand side of the QRS-complex T-130 (Template with 130 epoch length), the Zero-Template follows the average template instead of a straight line. Also, it can be observed that for T-150, the shape of the Zero-Template QRS-complex left hand side follows the average template as well, in this case it looks similar to a P-wave.

Three time domain examples of the Template Subtraction epoch of 50 (T-50), 100 (T-100), and 150 (T-150) sample range and its corresponding survey for a patient are shown in Fig. 16B. In red the raw LFP can be observed, showing R-peaks with high amplitudes. The signal coloured in black shows the filtered LFP after the template filtering, indicating strong R-peak suppression starting from approximately 0-20 V down to 0-10 V.

The voltage range observed for the filtered T-50, T-100, T-150 signals are comparable to the 0-10 V in the survey data *(Fig. 16A)*. Some outliers can be seen the survey data. For instance the peak around the 500th sample seems to be missing in the T-50, T-100 and T-150 time domain plots, possibly indicating a slight over-suppression of the signal.

J. Simulated LFP Signals with ECG artefacts

As only 9 LFPs with consistent ECG artefact were included for this study, we decided to add simulated data. In order to obtain this simulated data, we used simulated LFPs based on:

1) 54 LFP survey recordings (20 sec)
2) 9 external ECG measurements (20 sec)
3) 11 levels of contamination (100-1100 %)

In total we generated 5346 simulations, which were used in each of the 14 models for performance assessment. We used their corresponding survey data as a reference.

K. Analysis

To improve the analysis apart from the time domain, we have transformed the filtered LFPs into the frequency domain. To obtain their PSD's using the Welch's method, we have used a time window of 250 samples with 50 % overlap. As the beta-range is assumed to serve as the main range of interest, we have chosen this range for performance analysis. We have taken the distance between in the beta-range for analysis, illustrated in Fig. 17.

Using the survey data as reference, we have calculated an absolute percentage difference in both the time and frequency domain using 2 and 3. We have matched the chosen contact pairs for streaming and survey for a qualitative reference.

$$abs\% = \sqrt{\frac{PSD(LFP-fil) - PSD(LFP-sur)}{PSD(LFP-sur)} * 100}^{2} \quad (2)$$

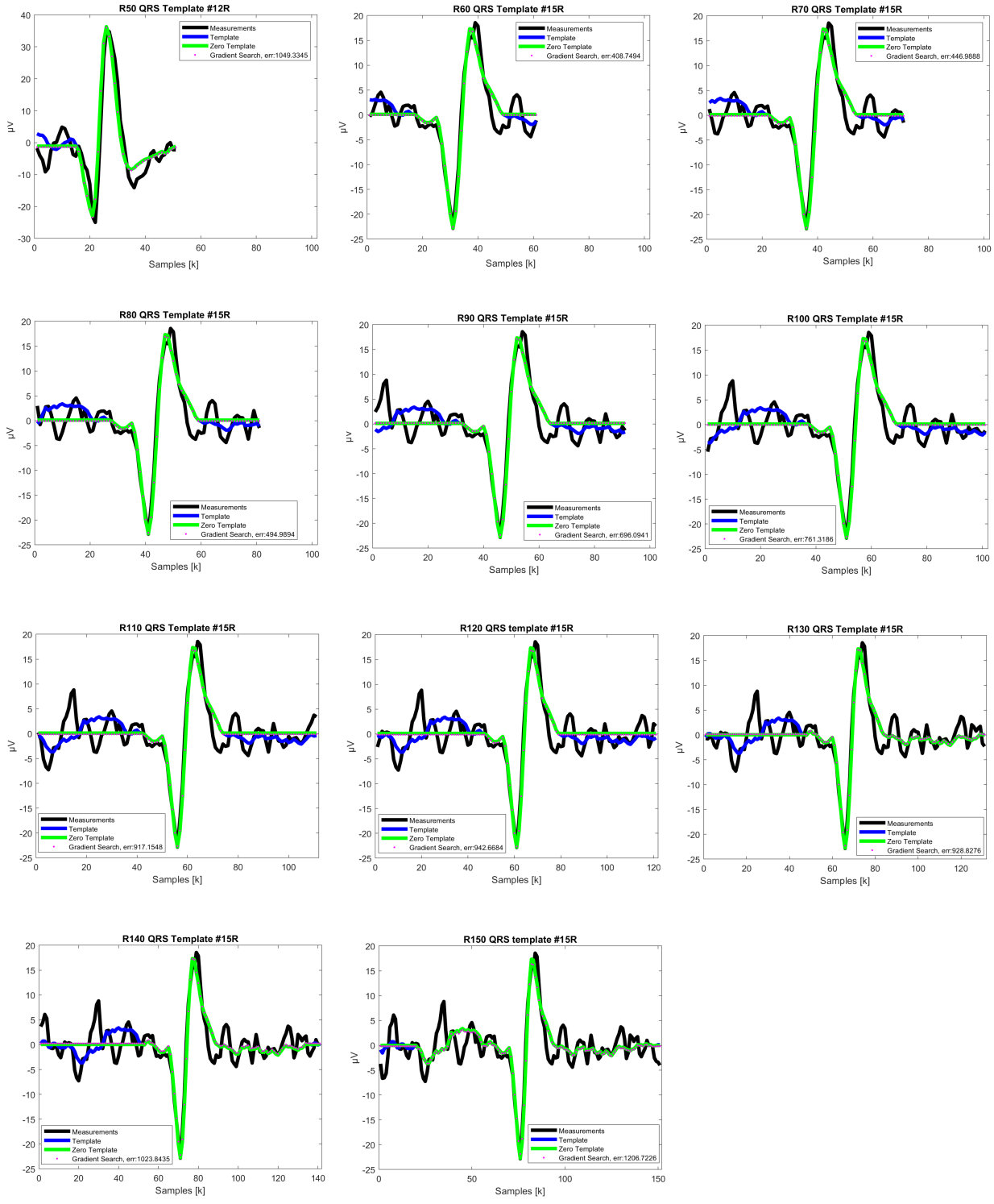

Figure 15: Figure showing the examples of 11 Template Subtraction QRS-complex epochs. In the black colour, the measured LFP is shown. The blue colours shows the estimated average QRS-complex template per channel. The Zero-Template, including tail deflection is shown in the green colour.

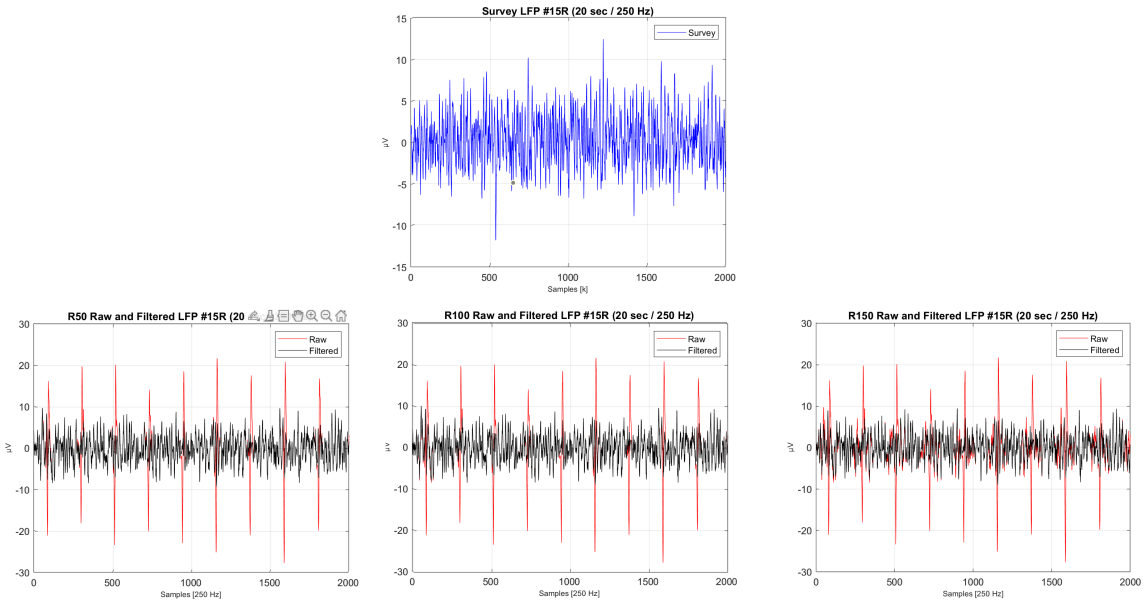

Figure 16: Figure showing a zoomed-in time window of an example survey LFP and three corresponding template subtraction results (T-50, T-100, T-150). In red, the LFP shows significant R-peaks. In black, all three template variations show strongly reduced R-peaks in the filtered LFP signal.

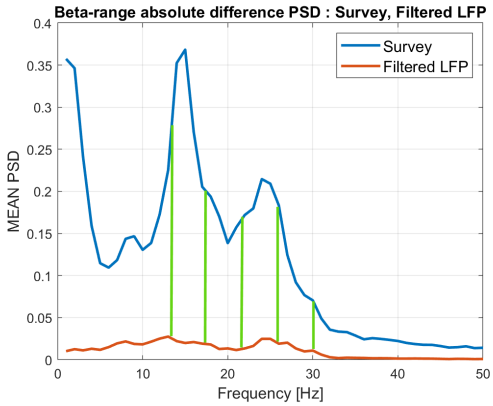

Figure 17: Illustration of calculating the difference between the filtered and the survey data in the beta-range (13-30 Hz). The green area resembles the range that is included for the performance calculation. We have used the distance between the signal points to calculate an absolute percentage difference.

$$abs\% = \sqrt{\frac{(LFP - fil) - (LFP - sur)}{(LFP - sur)} * 100}^{2} \quad (3)$$

Where LFP-fil is the filtered LFP and LFP-surv is survey LFP. We have calculated the differences of LFPs on per personal channel (#1), per group average (#9) and per simulations (#5346).

Abbreviated, we have implemented old (Perceive and T-100) and new (Zero-Peak, Autopeak, T-50:150) methods for performance analysis. For the adaptive methods, the measured ECG has been used for noise cancellation filtering. Survey data has been used for reference of all model performances. Per LFP, we have calculated the absolute difference in both the frequency (beta-range) and time domain. Outcomes are divided into three levels; personal, patient group and simulations.

3. Results

This section outlines the results of the analysis on the filtered LFPs per model. The average PSD's of the models were visually compared to three PSD, namely the original LFP PSD, survey PSD and Perceive PSD. First, the PSD plots resulting out of the adaptive filters will be compared. Then, the PSD plots of the template models will be assessed. Finally, the results for all three different data groups (#1, #9, #5346) are discussed by means of summarized tables (Table III).

A. Zero-Delay and Autopeak

Using the survey PSD (dark blue) as a reference, the raw LFP signal (red) shows significant masking of the beta-range (Fig. 18). Both Zero-Delay and Autopeak adaptive filtering methods do not bring any significant improvement in resurfacing the expected beta-peaks. As can be seen in Fig. 18, these two methods have not only an overly strong suppression of the LFP signal in the beta-range but also no significant difference between their PSD's.

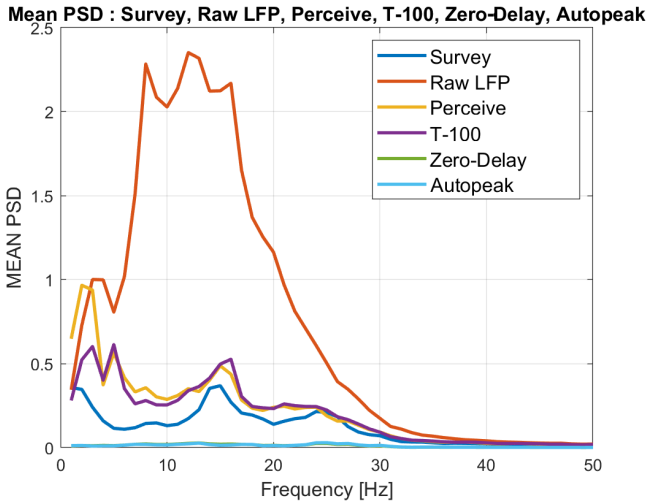

Figure 18: Graph showing the Mean PSD (9) of; survey (dark blue), raw LFP (red), compared to the results of Perceive, original T-100, Zero-Delay and Autopeak.

As these explored adaptive methods do not bring any improvements, we have returned to the perceive and original template method that still show higher resembles of the expected beta peaks. After visual inspection they seem to a more attractive approach.

B. Template Subtraction Results

The PSD analysis of the group average for all 11 variations are shown in Fig. 19. Compared to the raw LFP, all template variatios show significant suppression of the ECG noise (Fig 19 upper). Notably, focusing on the comparison of the template variations with only the survey in Fig 19 lower, the template variation PSDs show considerable differences in the lower frequencies. Furthermore, slight beta-range differences can be seen, but the lines mostly overlap. But all variations show a significant beta peak around 15 Hz and an attenuated second beta peak around 25 Hz. Compared to the original T-100, no significant differences can be visually observed.

C. Absolute Difference in PSD and Time

Additionally to the visual findings, the absolute differences per model in the time and PSD beta-range between the filtered LFP and the survey data calculated by 2 and 3.

All numerical results of the three levels have been documented in Table III. Their comparisons show unique differences on every level. For every outcome, the lowest absolute difference, and thus highest performance, is highlighted in green. Further analysis is done for the outcomes on each level, starting with an analysis in the frequency domain and afterwards in the time domain.

1) Personal Results

In the matrix of personal outcomes in the frequency domain, the highest accuracy for 5 out of 9 LFP channels is obtained

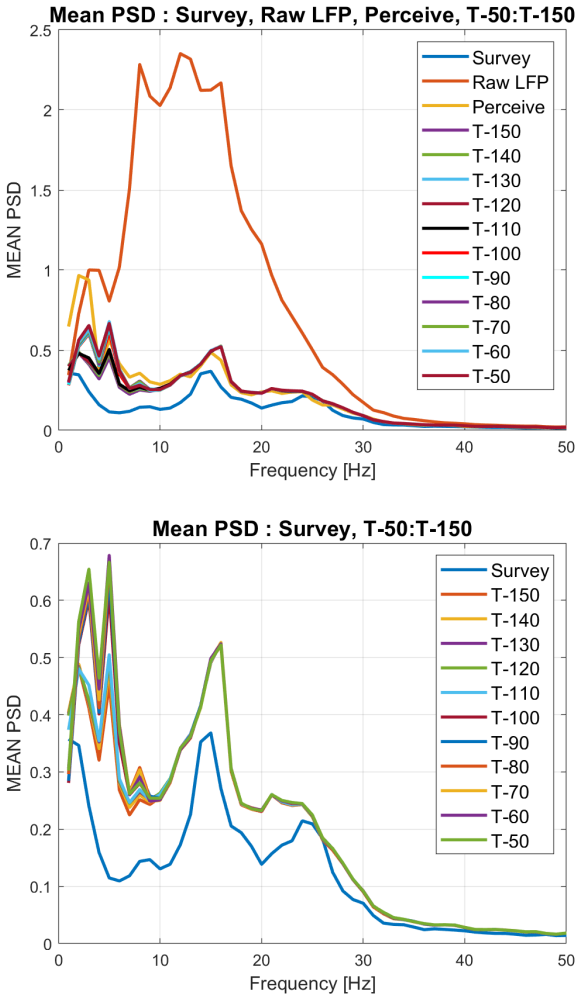

Figure 19: Upper: Graph showing the Mean PSD (9) of; Survey, raw LFP in red, compared to the result of Perceive and 11 Template variations. Lower: Graph showing the Mean PSD (9) of Survey and and 11 Template variations.

using the Perceive Toolbox, as seen in Table III-a. The T-140 gives the highest accuracy in twice and the T-150 and T-60 only once. For channel L18, the accuracy improvement between Perceive and T-140 is 0.6 %. Likewise for channel R14 (T-150) is 8.1% *(Fig.21)* and R18 (T-140) is 37.6% *(Fig.22)*.

In the time domain in the matrix of personal outcomes of Table III-b, all methods shows a performance spread of around50 % for all LFP channels. Only one channel shows optimal performance using the Perceive toolbox. T-100 (48.3%, 49,2%) and T-140 (48,35%, 46,31%) both show the optimal performance of 2 channels.

These results advocate that an improvement of ECG noise suppression can be made by choosing an optimal filter method. This suggest that the survey data can be used for personal

A.

abs % PSD	Method	Autopeak	Zero-Delay	Perceive	T-50	T- 60	T-70	T-80	T-90	T-100	T-110	T-120	T-130	T-140	T-150
LFP channel															
L12		91.35	91.65	6.83	8.73	9.12	9.34	8.90	8.77	9.37	8.99	8.92	9.19	9.14	8.95
L13		87.20	87.63	13.72	36.98	36.33	36.59	36.32	36.42	36.42	36.26	36.30	35.15	35.08	35.22
L18		75.25	75.86	40.26	41.13	41.44	41.33	41.53	41.49	41.28	41.37	41.18	39.80	39.67	39.84
R11		96.32	96.39	19.44	21.16	21.05	21.07	21.09	21.15	21.04	21.09	21.11	21.09	21.06	21.12
R12		98.07	96.82	0.63	36.98	36.33	36.59	36.32	36.42	36.42	36.26	36.30	35.15	35.08	35.22
R13		26.68	28.89	4.60	71.01	70.35	71.25	70.32	70.98	70.64	70.79	70.82	70.56	70.68	71.04
R14		96.64	94.83	41.18	36.05	36.05	36.11	36.05	36.08	36.08	35.98	36.14	36.14	33.12	33.11
R15		92.83	93.07	9.86	8.49	8.23	8.31	8.58	8.38	8.34	8.39	8.37	8.36	8.59	8.69
R18		63.92	65.00	49.36	13.19	12.52	12.51	12.78	12.62	12.28	12.60	13.01	12.01	11.76	11.87
Group Mean		80.92	81.13	20.65	30.41	30.16	30.35	30.21	30.26	30.21	30.19	30.24	29.72	29.35	29.45
Simulations		60.44	69.80	4.71	8.29	8.16	8.03	7.96	7.86	7.75	7.76	7.81	7.82	7.90	7.94

B.

abs % time	Method	Autopeak	Zero-Delay	Perceive	T-50	T-60	T-70	T-80	T-90	T-100	T-110	T-120	T-130	T-140	T-150
LFP channel															
L12		49.91	49.90	49.45	49.23	49.24	49.24	49.26	49.32	49.38	49.32	49.43	49.38	49.43	49.45
L13		50.14	50.14	54.45	53.37	52.99	53.17	53.52	54.03	54.94	54.29	53.95	53.36	52.46	51.87
L18		49.72	50.21	48.69	48.64	48.76	48.75	48.83	48.90	48.84	48.94	48.95	48.89	48.91	48.90
R11		49.89	49.87	49.36	49.76	49.62	49.59	49.61	49.73	49.75	49.92	50.00	49.72	49.68	49.46
R12		49.89	49.47	48.47	49.69	49.74	49.68	49.47	49.19	48.79	48.78	48.69	48.46	48.35	48.72
R13		49.92	49.82	46.74	47.09	47.17	47.09	47.01	47.11	47.03	46.86	47.00	47.12	46.31	46.32
R14		50.41	50.41	48.38	48.48	48.45	48.48	48.57	48.48	48.44	48.37	48.35	48.36	48.68	48.71
R15		50.86	50.85	48.80	48.37	48.22	48.37	48.35	48.31	48.27	48.35	48.42	48.48	48.38	48.34
R18		50.08	50.08	49.30	49.93	49.95	49.78	49.75	49.42	49.21	48.98	48.88	48.96	49.22	49.39
Group Mean		50.09	50.08	49.29	49.40	49.35	49.35	49.37	49.39	49.41	49.31	49.30	49.19	49.05	49.02
Simulations		33.19	45.96	9.27	4.38	4.53	4.65	4.78	4.92	5.03	5.11	5.19	5.29	5.35	5.39

Table III: A) Subtable showing the outcomes of the absolute PSD % (beta-range) difference for all data groups. B) Subtable showing the outcomes of the absolute time % difference for all data groups. In green the outcome with the highest performance is highlighted for all data groups.

tweaking of ECG noise suppression calibration.

2) Patient Group Results

At the level of the patient group (9), the frequency domain analysis shows an absolute mean difference of 80.92% for Autopeak and 81.13% for Zero-Delay respectively. The model with the lowest difference and thus highest accuracy is the Perceive toolbox with an absolute difference of 20.7%. Compared to the original T-100 (30,21%), the Perceive toolbox shows an overall accuracy improvement of 9,5%. Within the template variations, the highest found group accuracy is 29.35%, which is an improvement of 0.86% over the original T-100.

In the time domain, the Autopeak and Zero-Delay methods show the highest absolute difference with 50,08% and 50,08% respectively. The lowest absolute difference is obtained for the T-150 with 49.01%. Compared to the original T-100 (49.41%) this is an accuracy improvement of 0.4%. Within the template variations, no outstanding performance differences can be found. Compared to the Perceive toolbox with 49,29%, the T-150 shows an accuracy improvement of 0.27%.

3) Simulation Results

At the level of the simulated data, the frequency domain analysis shows that the adaptive methods have the lowest accuracy with an absolute difference of 60,44% and 69,8% for the Autopeak and Zero-Delay respectively. The Perceive outcomes shows the highest performance with an absolute difference of 4.7%. The performance of the 11 template variations are spread between 7.75-8.29%.

In the time domain, the highest performance accuracy is found for T-50 with 4.3%, whereas Perceive has 9.3%. Autopeak and Zero-Delay give 33,2% and 45.6%. T-150 shows the lowest template variation accuracy in time domain with 5.4%.

4. Conclusion

The first conclusion is that both the Adaptive Zero-Delay and Autopeak were able not able to adequately suppress the ECG artefact without losing the beta-peaks. This be substantiated by each of the three data groups in time and frequency domain. Both adaptive filter methods show no good estimation of the ECG component in the raw LFP signal. Possibly this can be explained due to the fact that these methods are based on minimizing the squared error based on every time a new sample. They seem to be too sensitive to the

amplitude fluctuations of the QRS-complex. The quality of the estimated noise component is crucial for the quality of the output signal. Notably, as the ECG signal is very pronounced, even step function like, the template subtraction method is more appropriate than the adaptive filters per sample input.

The second conclusion is that the used adaptive filters seem to be more suitable to more stationary signals with less amplitude fluctuations in time. These observations on the adaptive methods suggest that subtraction of noise from the raw signal poses a risk of signal distortion by creating even additional noise. This could explain the bad performance of these adaptive filters.

The third conclusion is that on a personal level, in the frequency domain, upside potential might be up to 37.6 % improvement as compared to the Perceive toolbox being the benchmark. This conclusion contradicts with the aim of aDBS to find an universal method.

The fourth conclusion is that on the other two levels, the group level and the simulated level, no clear difference in outcomes could be identified between the template variations.

The fifth and last conclusion is that the Perceive toolbox shows the best ECG noise suppression performance for both the group and simulated levels. For the patient group the Perceive shows an improvement of approximately 10 % over the various template subtraction methods. For the simulated data the Perceive toolbox shows a performance improved of approximately 3% over the template subtraction methods.

5. Discussion & Recommendations

This section outlines various observations and recommendations from my side.

A. Exploring other Adaptive Filters

First of all, this project scope as initially defined falls short into exploring other adaptive filters such as pattern recognition and neural net adaptive filters. In hindsight, in general these filters are more suitable for signals with characteristic pattern repetition, such as the ECG. Notably, we have used the PADASIP NLMS Adaptive filter toolbox that requires a random weighting factor. To counteract the randomness of this approach, we have arbitrarily selected a 1000 calculations to estimate the noise component.

It can be recommended to conduct further research regarding other adaptive filters such as pattern recognition and neural network to explore the potential of adaptive filters for ECG noise suppression within LFP data.

B. Critical influence of Time Synchronization

Secondly, this research was limited by the lacking accurate timestamps of the LFPs captured by the Medtronic Percept^{TM}. The default timestamp of this system is inadequate for reliable data synchronization of LFPs with other biometric data. Also we have found that an alternative synchronization method, the stimulation ramping approach, differs on each LFP streaming channel and required manual adjustment on thresholds. Thus this alternative synchronization method is prone to subjective error. As the outcomes of Adaptive Zero-Delay and Autopeak are based on this synchronization approach, it makes it very difficult to exclude the impact of inaccurate synchronization on the overall performance.

It can be recommended to explore and implement a reliable time synchronization method. This would improve the alignment of other properly timestamped biometric data. Only on the foundation of a reliable synchronization method, machine learning could accelerate the learning of biomarker identification and implementation.

C. Signal Lengths

Thirdly, as the length of the available survey data used for comparison was only 20 seconds, we had to limit ourselves to shorten the input signals to 20 seconds as well.

It can be recommended, to use longer time windows of survey and input data for a more accurate approximation of the performance of the ECG noise suppression methods.

D. Influence of Beta-Burts on PSD analysis

Fourthly, in this project, we have used Fourier transformation to analysis the signals in the frequency domain. However it has been found that a Fourier transform excludes the ability to analyse beta-bursts, that have been reported as a biomarker for movement loss [31]–[33].

It can be recommended to extend the research on ECG noise suppression models to find and highlight the beta-bursts.

E. Excluded Patient Biometrics

Lastly, another drawback of the scope of this project is that some obvious biometric data, such as gender or progressive state of PD, were not considered. This might be important as we identified personal tweaking as a more promising approach.

It is suggested to take into account various other biometric factors such as gender, progressive state and hormonal differences for a more in detail analysis. Apart from the used BrainSense^{TM} that measures locally, one could also the novel Medtronic SenSight^{TM} technology, that provides directional information as well [34], [35].

REFERENCES

[1] J. Jankovic, "Parkinson's disease: clinical features and diagnosis," *Journal of neurology, neurosurgery & psychiatry*, vol. 79, no. 4, pp. 368–376, 2008.

[2] M. Jakobs, A. Fomenko, A. M. Lozano, and K. L. Kiening, "Cellular, molecular, and clinical mechanisms of action of deep brain stimulation—a systematic review on established indications and outlook on future developments," *EMBO molecular medicine*, vol. 11, no. 4, p. e9575, 2019.

[3] "Neuromodulation," https://neurology.ufl.edu/divisions/epilepsy/neuromodulation-vns-rns-dbs/, note = University of Florida Health, Department of Neurology.

[4] J. M. Tan, E. S. Wong, and K.-L. Lim, "Protein misfolding and aggregation in parkinson's disease," *Antioxidants & redox signaling*, vol. 11, no. 9, pp. 2119–2134, 2009.

[5] S. Chiken and A. Nambu, "Disrupting neuronal transmission: mechanism of dbs?" *Frontiers in systems neuroscience*, vol. 8, p. 33, 2014.

[6] S. Miocinovic, S. Somayajula, S. Chitnis, and J. Vitek, "History, applications, and mechanisms of deep brain stimulation. jama neurol. 70 (2), 163–171," 2013.

[7] C. Bédard and A. Destexhe, "Macroscopic models of local field potentials and the apparent 1/f noise in brain activity," *Biophysical journal*, vol. 96, no. 7, pp. 2589–2603, 2009.

[8] P. E. Mosley and H. Akram, "Neuropsychiatric effects of subthalamic deep brain stimulation," in *Handbook of Clinical Neurology*. Elsevier, 2021, vol. 180, pp. 417–431.

[9] M. Parastarfeizabadi and A. Z. Kouzani, "Advances in closed-loop deep brain stimulation devices," *Journal of neuroengineering and rehabilitation*, vol. 14, no. 1, pp. 1–20, 2017.

[10] Y. Chen, C. Gong, Y. Tian, N. Orlov, J. Zhang, Y. Guo, S. Xu, C. Jiang, H. Hao, W.-J. Neumann *et al.*, "Neuromodulation effects of deep brain stimulation on beta rhythm: a longitudinal local field potential study," *Brain Stimulation*, vol. 13, no. 6, pp. 1784–1792, 2020.

[11] A. Højlund, M. V. Petersen, K. S. Sridharan, and K. Østergaard, "Worsening of verbal fluency after deep brain stimulation in parkinson's disease: A focused review," *Computational and Structural Biotechnology Journal*, vol. 15, pp. 68–74, 2017.

[12] O. Herreras, "Local field potentials: myths and misunderstandings," *Frontiers in neural circuits*, vol. 10, p. 101, 2016.

[13] M. M. N. Mannan, M. A. Kamran, and M. Y. Jeong, "Identification and removal of physiological artifacts from electroencephalogram signals: A review," *Ieee Access*, vol. 6, pp. 30 630–30 652, 2018.

[14] W.-J. Neumann, M. M. Sorkhabi, M. Benjaber, L. K. Feldmann, A. Saryyeva, J. K. Krauss, M. F. Contarino, T. Sieger, R. Jech, G. Tinkhauser *et al.*, "The sensitivity of ecg contamination to surgical implantation site in brain computer interfaces," *Brain stimulation*, vol. 14, no. 5, pp. 1301–1306, 2021.

[15] R. Panda, "Removal of artifacts from electrocardiogram," Ph.D. dissertation, 2012.

[16] "Basic ecg interpretation," https://slidetodoc.com/basic-ecg-interpretation-wendy-callaway-rn-bsn-cardiopulmonary/, note = .

[17] A. Eusebio, W. Thevathasan, L. D. Gaynor, A. Pogosyan, E. Bye, T. Foltynie, L. Zrinzo, K. Ashkan, T. Aziz, and P. Brown, "Deep brain stimulation can suppress pathological synchronisation in parkinsonian patients," *Journal of Neurology, Neurosurgery & Psychiatry*, vol. 82, no. 5, pp. 569–573, 2011.

[18] A. A. Kühn, F. Kempf, C. Brücke, L. G. Doyle, I. Martinez-Torres, A. Pogosyan, T. Trottenberg, A. Kupsch, G.-H. Schneider, M. I. Hariz *et al.*, "High-frequency stimulation of the subthalamic nucleus suppresses oscillatory β activity in patients with parkinson's disease in parallel with improvement in motor performance," *Journal of Neuroscience*, vol. 28, no. 24, pp. 6165–6173, 2008.

[19] W.-J. Neumann, F. Staub-Bartelt, A. Horn, J. Schanda, G.-H. Schneider, P. Brown, and A. A. Kühn, "Long term correlation of subthalamic beta band activity with motor impairment in patients with parkinson's disease," *Clinical Neurophysiology*, vol. 128, no. 11, pp. 2286–2291, 2017.

[20] N. V. Thakor, J. G. Webster, and W. J. Tompkins, "Estimation of qrs complex power spectra for design of a qrs filter," *IEEE Transactions on biomedical engineering*, no. 11, pp. 702–706, 1984.

[21] D. A. Wagenaar and S. M. Potter, "Real-time multi-channel stimulus artifact suppression by local curve fitting," *Journal of neuroscience methods*, vol. 120, no. 2, pp. 113–120, 2002.

[22] "Ecg artefact suppression and external data synchronization with the medtronic percept, a deep brain stimulator with sensing technology."

[23] "Github: Perceive toolbox," https://github.com/neuromodulation/perceive,.

[24] "Percept™ pc neurostimulator," https://www.medtronic.com/us-en/healthcare-professionals/products/neurological/deep-brain-stimulation-systems/percept-pc.html, note = Last updated October 2021.

[25] D. Satzer, D. Lanctin, L. E. Eberly, and A. Abosch, "Variation in deep brain stimulation electrode impedance over years following electrode implantation," *Stereotactic and functional neurosurgery*, vol. 92, no. 2, pp. 94–102, 2014.

[26] J. C. Williams, J. A. Hippensteel, J. Dilgen, W. Shain, and D. R. Kipke, "Complex impedance spectroscopy for monitoring tissue responses to inserted neural implants," *Journal of neural engineering*, vol. 4, no. 4, p. 410, 2007.

[27] "Fda gives green light to medtronic's dbs system with brain signal tracking," https://www.bioworld.com/articles/436061-fda-gives-green-light-to-medtronics-dbs-system-with-brain-signal-tracking?v=preview, note = Published: June 25, 2020.

[28] H. Yuk, B. Lu, and X. Zhao, "Hydrogel bioelectronics," *Chemical Society Reviews*, vol. 48, no. 6, pp. 1642–1667, 2019.

[29] M. H. Hayes, "Statistical digital signal processing and modeling. john wiley&sons," *New York*, 1996.

[30] M. Cejnek, "Padasip—open source library for adaptive signal processing in language python," *Studentská Tvurcí cinnost*, 2017.

[31] M. C. Vinding, P. Tsitsi, J. Waldthaler, R. Oostenveld, M. Ingvar, P. Svenningsson, and D. Lundqvist, "Reduction of spontaneous cortical beta bursts in parkinson's disease is linked to symptom severity," *Brain communications*, vol. 2, no. 1, p. fcaa052, 2020.

[32] G. Tinkhauser, A. Pogosyan, S. Little, M. Beudel, D. M. Herz, H. Tan, and P. Brown, "The modulatory effect of adaptive deep brain stimulation on beta bursts in parkinson's disease," *Brain*, vol. 140, no. 4, pp. 1053–1067, 2017.

[33] R. Lofredi, H. Tan, W.-J. Neumann, C.-H. Yeh, G.-H. Schneider, A. A. Kühn, and P. Brown, "Beta bursts during continuous movements accompany the velocity decrement in parkinson's disease patients," *Neurobiology of disease*, vol. 127, pp. 462–471, 2019.

[34] "Fda approves first-of-its-kind sensight™ directional lead system for dbs therapy," https://news.medtronic.com/2021-06-07-FDA-Approves-First-of-its-Kind-SenSight-TM-Directional-Lead-System-for-DBS-Therapy,.

[35] T. A. Dembek, P. Reker, V. Visser-Vandewalle, J. Wirths, H. Treuer, M. Klehr, J. Roediger, H. S. Dafsari, M. T. Barbe, and L. Timmermann, "Directional dbs increases side-effect thresholds—a prospective, double-blind trial," *Movement Disorders*, vol. 32, no. 10, pp. 1380–1388, 2017.

APPENDIX. A

Longitudinal recordings in patients implanted with DBS electrodes — **VISIT 1 STIM OFF**

Patient Identificatie Nummer: | P | D |_|_|_|_| — **Onderzoeker: |_|_|**

Brainsense meting STIM OFF en ON

Instellen BrainSense met gewenste frequenty en pulse width, 0 mA!

Instrueer de patiënt niet te spreken tijdens de meting.

Gebruik "Start" en "Stop" triggers TMSi per taak!

- ☐ 1 minuut rust
- ☐ 30 seconden statisch bewegen (vingers en pols RECHTS in hyperextensie)
- ☐ 10 seconden rust
- ☐ 30 seconden statisch bewegen (vingers en pols LINKS in hyperextensie)
- ☐ 10 seconden rust
- ☐ 30 seconden tappen RECHTS (wijsvinger op duim tappen RECHTS)
- ☐ 10 seconden rust
- ☐ 30 seconden tappen LINKS (wijsvinger op duim tappen LINKS)
- ☐ 10 seconden rust
- ☐ 30 seconden dynamisch bewegen (RECHTERhand open-dicht knijpen)
- ☐ 10 seconden rust
- ☐ 30 seconden dynamisch bewegen (LINKERhand open-dicht knijpen)
- ☐ 10 seconden rust
- ☐ 30 seconden dynamisch bewegen (RECHTERhand pro/supinatie)
- ☐ 10 seconden rust
- ☐ 30 seconden dynamisch bewegen (LINKERhand pro/supinatie)
- ☐ 10 seconden rust
- ☐ 30 seconden intentionele bewegingen (vinger onderzoeker – neus patiënt RECHTS)
- ☐ 10 seconden rust
- ☐ 30 seconden intentionele bewegingen (vinger onderzoeker – neus patiënt LINKS)
- ☐ 10 seconden rust
- ☐ 30 seconden spraak (tekst oplezen)
- ☐ 10 seconden rust
- ☐ 30 seconden stappen op de plaats (indien mogelijk)
- ☐ 10 seconden rust

BrainSense meting en TMSi meting **CONTINUEREN, NIET PAUZEREN!** *Maar let op: max. 30 min streamen.*

Longitudinal recordings in patients implanted with DBS electrodes — **VISIT 1** — **STIM ON**

Patient Identificatie Nummer: | P | D |_|_|_| — **Onderzoeker: |_|_|**

Amplitude (mA) langzaam opvoeren per electrode tot aan gewenste effect (of pre-operatief bepaald mA)
Instellingen Percept:

Rechts
mA _____ Frequency _____ Pulse width _____

Links
mA _____ Frequency _____ Pulse width _____

BrainSense meting met stimulatie aan

Instrueer de patiënt niet te spreken tijdens de meting.

Gebruik "Start" en "Stop" triggers TMSi per taak!

- ☐ 1 minuut rust
- ☐ 30 seconden statisch bewegen (vingers en pols RECHTS in hyperextensie)
- ☐ 10 seconden rust
- ☐ 30 seconden statisch bewegen (vingers en pols LINKS in hyperextensie)
- ☐ 10 seconden rust
- ☐ 30 seconden tappen RECHTS (wijsvinger op duim tappen RECHTS)
- ☐ 10 seconden rust
- ☐ 30 seconden tappen LINKS (wijsvinger op duim tappen LINKS)
- ☐ 10 seconden rust
- ☐ 30 seconden dynamisch bewegen (RECHTERhand open-dicht knijpen)
- ☐ 10 seconden rust
- ☐ 30 seconden dynamisch bewegen (LINKERhand open-dicht knijpen)
- ☐ 10 seconden rust
- ☐ 30 seconden dynamisch bewegen (RECHTERhand pro/supinatie)
- ☐ 10 seconden rust
- ☐ 30 seconden dynamisch bewegen (LINKERhand pro/supinatie)
- ☐ 10 seconden rust
- ☐ 30 seconden intentionele bewegingen (vinger onderzoeker – neus patiënt RECHTS)
- ☐ 10 seconden rust
- ☐ 30 seconden intentionele bewegingen (vinger onderzoeker – neus patiënt LINKS)
- ☐ 10 seconden rust
- ☐ 30 seconden spraak (tekst oplezen)
- ☐ 10 seconden rust
- ☐ 30 seconden stappen op de plaats (indien mogelijk)
- ☐ 10 seconden rust

APPENDIX. B

```
# -*- coding: utf-8 -*-
"""
Created on Mon Nov 29 16:28:24 2021

@author: palla
"""


from __future__ import division
import numpy as np
import matplotlib.pylab as plt
import padasip as pa
import scipy.io as sio
from numpy import save
from scipy.signal import find_peaks

#spectral density tools
from scipy import signal

def pknorm(x, mvalue, stdvalue):
    xo = (x - mvalue)/stdvalue
    return xo

def znorm(x, axis=0):
    meanval = np.mean(x, axis)
    stdval  = np.std(x, axis)
    xo = pknorm(x, meanval, stdval)
    return xo

#A. loading and preprocessing of mat files into python


fs = 250
fullortask = '.task1.'
fullortaskkey = 'task1'
namepatient = 'PD'
chosenLFP = 'LFP'
folder = "C:/"
patient =  str(namepatient) + str(fullortask)

ECG_ = sio.loadmat(folder + patient + 'ECG.mat')

LFP_L = sio.loadmat(folder + patient + 'LFPL.mat')
LFP_R = sio.loadmat(folder + patient + 'LFPR.mat')

#taking right key out of dict
ECG = ECG_[str(namepatient)+str(fullortaskkey)+"ECG"].T
LFP_L = LFP_L[str(namepatient)+str(fullortaskkey)+"LFPL"].T
LFP_R = LFP_R[str(namepatient)+str(fullortaskkey) +"LFPR"].T

ECGinverse = ["PD010"]

if str(namepatient) in ECGinverse:
    ECG = ECG[np.logical_not(np.isnan(ECG))]
else:
    ECG = -ECG[np.logical_not(np.isnan(ECG))]

LFP_L_whole = LFP_L[np.logical_not(np.isnan(LFP_L))]
LFP_R_whole = LFP_R[np.logical_not(np.isnan(LFP_R))]

LFP_L = LFP_L_whole[0:5000]
LFP_R = LFP_R_whole[0:5000]

ECG = ECG[0:5000]

if str(chosenLFP) == 'LFP_L_OFF':
```

```
    LFP = LFP_L
else:
    LFP = LFP_R

ECG_squeeze = np.squeeze(ECG)
ECG_prehp = ECG_squeeze
time_ECG_prehp = len(ECG)/fs


# highpass filter of 1 hz
t = np.linspace(0, time_ECG_prehp, len(ECG_prehp), False)
b, a = signal.butter(4, 1, 'high', analog=True)
w, h = signal.freqs(b, a)
plt.semilogx(w, 20 * np.log10(abs(h)))
plt.title('Butterworth filter frequency response')
plt.xlabel('Frequency [radians / second]')
plt.ylabel('Amplitude [dB]')
#plt.margins(0, 0.1)
plt.grid(which='both', axis='both')
plt.axvline(1, color='green') # cutoff frequency
plt.show()


fig, (ax1, ax2) = plt.subplots(2, 1, sharex=True)
ax1.plot(ECG_prehp)
#x2.axis([0, 1 -2, 2])
ax1.set_xlabel('samples [k] ')
sos = signal.butter(6, 1, 'hp', fs=250, output='sos')
ECG_posthp = signal.sosfiltfilt(sos, ECG_prehp)
ax2.plot(ECG_posthp)
ax2.set_title('After 1 Hz high-pass filter')
#ax2.axis([0, 1, -2, 2])
ax2.set_xlabel('samples [k] ')
plt.tight_layout()
plt.show()

A = 0
B = len(LFP)

LFP_squeeze = np.squeeze(LFP)

LFP_norm = znorm(LFP_squeeze)
ECG_norm = znorm(ECG_posthp)

LFP_range = LFP_norm[A:B]
ECG_range = ECG_norm[A:B]

#B. Extended part for Adaptive Autopeak.

#detect R-peaks

flag_peak = 0

data = np.squeeze(ECG_norm)
rpeaks, _= find_peaks(data, height=2)
plt.plot(data)
height_r_ECGpeaks =data[rpeaks]
plt.plot(rpeaks, data[rpeaks], "x")
plt.plot(np.zeros_like(data), "--", color="brown")
plt.show()

data = np.squeeze(-ECG_norm)
speaks, _= find_peaks(data, height=2)
plt.plot(data)
height_s_ECGpeaks =data[speaks]
plt.plot(speaks, data[speaks], "x")
plt.plot(np.zeros_like(data), "--", color="brown")
```

```
plt.show()

meanheightsecgspeaks = np.mean(height_s_ECGpeaks)
meanheightsecgrpeaks = np.mean(height_r_ECGpeaks)

# Determine orientation R/S peaks
if np.mean(height_s_ECGpeaks) > np.mean(height_r_ECGpeaks):
   rpeaks = speaks;
   flag_peak = 1
else:
   data = ECG_range

print("flagpeak =" +str(flag_peak))

locs = rpeaks

locs_lfp = []
peak1_val = []
peak1_idx = []
peak2_val = []
peak2_idx = []


if locs[0] <= 20:
   locs[1:]
if locs[-1] >= (len(data)-20):
   locs[:-2]

if locs[0] <= 20:
   locs[1:]
if locs[-1] >= (len(data)-20):
   locs[:-2]

if locs[0] <= 20:
   locs[1:]
if locs[-1] >= (len(data)-20):
   locs[:-2]

interval = np.transpose(locs)

intervala = []
intervalb= []

# Determine start and end of interval
for i in range(len(interval)):
   intervala.append(interval[i]-20)
   intervalb.append(interval[i]+20)

intervalzip = list(zip(intervala,intervalb))

column = []
for i in range(len(intervalzip)):
  column.append(LFP_range[intervala[i]:intervalb[i]])

for i in range(len(intervalzip)):

   peak1_val.append(np.amax(column[i]))
   peak1_idx.append(np.where(column[i] == np.amax(column[i])))
   peak2_val.append(np.amin(column[i]))
   peak2_idx.append(np.where(column[i] == np.amin(column[i])))

peak1_val = np.squeeze(peak1_val)
peak1_idx = np.squeeze(peak1_idx)
peak2_val = np.squeeze(peak2_val)
peak2_idx = np.squeeze(peak2_idx)
```

```
if np.mean(abs(peak1_val)) > np.mean(abs(peak2_val)):
    locs_lfp = locs -20 + peak1_idx
    flag_peak = 0

else:
    locs_lfp = locs -20 + peak2_idx
    flag_peak = 1


meandifferencelocs = np.mean(locs_lfp-locs)

#idenitfy delay value
C = int(meandifferencelocs)
#C= 0 (for Adaptive d0 C=0)


# C. Preprocess for Adaptive NLMS filer

lenLFPminint = len(LFP)-1

#C. equalize lengths for adaptive NLMS input
LFP_syn = LFP_squeeze[1+C:lenLFPminint+C-1]
ECG_syn = ECG_posthp[1:lenLFPminint-1]

LFP_norm = znorm(LFP_syn)
ECG_norm = znorm(ECG_syn)

A = 0
B = len(LFP_norm)

#-3 to equalize lengths due to matrix of 4 input
ECG_range = ECG_norm[A:B]
LFP_range = LFP_norm[A:B-3]


mu = 0.001


xinput = pa.input_from_history(ECG_range, 4) # input ECG
dinput= LFP_range

input_y = []
input_e = []
input_w = []


#D. NLMS Adaptive Noise Cancellation Filter
for i in range(1000):
    f = pa.filters.FilterNLMS(n=4, mu=0.001, w="random")
    y_i, e_i, w_i = f.run(dinput, xinput)
    input_y.append(y_i)
    input_e.append(e_i)
    input_w.append(w_i)


y_arr  = np.array(input_y)
e_arr = np.array(input_e)
w_arr = np.array(input_w)

y = np.average(y_arr, axis=0)
e = np.average(e_arr, axis=0)
w = np.average(w_arr, axis=0)
```